Neuron, volume *77*

Supplemental Information

Developmental Refinement of Vesicle Cycling at Schaffer Collateral Synapses

Tobias Rose, Philipp Schoenenberger, Karel Jezek, and Thomas G. Oertner

Inventory of Supplemental Information

Supplemental Experimental Procedures

Supplemental References

Figure S1: Localization of Ratio-sypHy. This figure is related to Figure 1, it provides additional information about the vesicular localization of the indicator.

Figure S2: Synaptic topology in dissociated and slice culture. This figure is related to Figure 2. It illustrates the orthogonal organization of axons and dendrites in CA1 and the parallel growth of axons and dendrites in dissociated culture, resulting in multiple, extremely strong synaptic connections.

Figure S3: Analysis of ratio-sypHy fluorescence decay. This figure is related to Figure 4. We analyzed the fluorescence decay in more detail, fitting a two-step model of endocytosis/reacidification. The fit, however, was not improved compared to a single exponential fit. Our conclusion: reacidification is much faster than endocytosis. We need to show this data to explain and justify our comparative analysis in the main manuscript.

Figure S4: Alkaline trapping experiment at the same set of boutons. This figure is related to Figure 5. An experiment is shown where all steps of the alkaline trapping experiments were performed on the same boutons, which is the standard procedure in dissociated culture.

Figure S5: Correction for spontaneous alkalization. This figure is related to Figure 6.
It provides additional information about a potential source of error in the pool size estimates and our correction algorithm.

Figure S6: Chronic depolarization does not change total vesicle cluster size.
This figure is related to Figure 7: An important control experiment to exclude that overnight depolarization reduces the total number of vesicles.

CA3_timestamps.zip Spike train data recorded in vivo (ASCII). Essential to reproduce our experiments.

SUPPLEMENTAL EXPERIMENTAL PROCEDURES

Preparation and transfection of hippocampal slices and dissociated cultures

Organotypic hippocampal slices were prepared from Wistar rats at p5 as described (Stoppini et al., 1991), in accordance with the animal care and use guidelines of the Veterinary Department Basel-Stadt. Briefly, dissected hippocampi were cut into 350 µm slices with a tissue chopper (McIllwain) and placed on a porous membrane (Millicell CM, Millipore). Cultures were maintained at 37°C, 5% CO_2 in a medium containing 80% MEM (Gibco 32360), 20% horse serum (Gibco 16050) supplemented with 1mM L-glutamine, 0.00125% ascorbic acid, 0.001 mg/ml insulin, 1mM $CaCl_2$, 2 mM $MgSO_4$, 13 mM D-glucose and 1 µM retinol. Cultures were transfected at DIV 5-7 ('mature') or DIV 1-2 ('immature') and experiments were performed either 1-3 weeks ('mature') or 5-7 days ('immature') after targeted transfection of CA3. To selectively transfect neurons in CA3, we constructed a targeting apparatus that allowed us to center a glass capillary (Ø 0.84 mm) at a defined distance (8 mm) over CA3. By fixing a gene gun (Helios, BioRad) 19 mm over the capillary and shooting through this aperture, we were able to limit the ballistic spread of DNA-coated gold particles (diameter 1.6 µm, 2.5 µg DNA per mg gold, BioRad) to a target area of ~0.8 mm diameter, typically transfecting 1-4 CA3 pyramidal cells.

Dissociated hippocampal cultures were prepared from E18 Wistar rats. Hippocampi were isolated in ice-cold Hank's salt solution and dissociated using trypsin-EDTA (0.05% for 5-10 min). Neurons were suspended in MEM plus glutamax (Gibco 41090, supplemented with 11% fetal calf serum and 16.6 mM D-glucose). 50% of the plated cells were transfected by electroporation (Nucleofector, Amaxa). We plated neurons on poly-L-lysine-coated glass cover slips at a density of ~300-500 cells/mm^2. Cultures were maintained in Neurobasal medium supplemented with 2% B27 (Invitrogen), 0.5 mM L-glutamine, 0.9 U/ml penicillin and 0.9 µg/ml streptomycin. Experiments were carried out between DIV 17 and 26 (typically DIV 20).

Construction of Ratio-sypHy

The cDNA encoding for synaptophysin I (sypI) with a single pHluorin moiety fused after its third transmembrane domain was amplified by PCR, excluding the stop codon and introducing an N-terminal *AvrII* and a C-terminal *NotI* restriction site in the process. The product was cut with *AvrII* / *NotI* and

inserted into a neuron-specific synapsin-I (syn) promoter vector in frame with the RFP tdimer2(12) using *NheI / NotI*. The fusion of unmodified sypI with tdimer2 was generated by PCR amplification of sypI from a sypI-mRFP fusion construct (indroducing NheI and NotI sites), followed by insertion into the same tdimer2 target vector as above. (Primers: ratio-sypHy, 5'-GCGC *CCTAGG* TTTAAACGGGCCCTCTAGAC-3', 5'-ATT *GCGGCCGC* GGCGTAATCGGGCACA-3'; syp-tdimer2, 5'-ATT *GCTAGC* AGGCATGGACGTGGTGAA-3', 5'-ATT *GCGGCCGC* CATCTGATTGGAGAA-3'). Constructs were amplified and purified using MaxiPrep Kits (Qiagen) and verified by DNA sequencing. The construct used in this study (ratio-sypHy) and a further version containing two intravesicular pHluorin moieties (ratio-sypHy2x) are available on addgene (www.addgene.com).

Solutions and electrophysiology

Hippocampal slice cultures were placed in the recording chamber of the microscope and superfused with artificial cerebrospinal fluid (ACSF) containing (in mM): 127 NaCl, 2.5 KCl, 2 $CaCl_2$, 1 $MgCl_2$, 25 $NaHCO_3$, 1.25 NaH_2PO_4 and 25 D-glucose. For ratio-sypHy calibration we employed two different approaches. For weak base calibration experiments (Roos and Boron, 1981), 50mM NaCl was substituted by an equimolar amount of NH_4Cl. For protonophore calibration we used a nominally Ca^{2+}-free solution mimicking intracellular cation concentrations to allow for the electroneutral exchange of H^+, Na^+, and K^+ ions. The solution contained (in mM): 129.5 KCl, 3 $MgCl_2$, 18.25 choline bicarbonate, 6.75 $NaHCO_3$, 1.25 NaH_2PO_4, and 25 glucose. The protonophores nigericin and monensin were used at a final concentration of 10 and 40 µM. All extracellular solutions were gassed with 95% O_2, 5% CO_2 to a pH of 7.4. To block recurrent excitation during electrical stimulation and prevent NMDA receptor-dependent long-term plasticity, 10 µM 2,3-Dioxo-6-nitro-1,2,3,4-tetrahydrobenzo[f]quinoxaline-7-sulfonamide (NBQX, Tocris) and 10 µM 3-((R)-2-Carboxypiperazin-4-yl)-propyl-1-phosphonic acid (*R*-CPP, Tocris) were always added to the ACSF. Non-aqueous stock solutions of pharmacological agents were prepared either in DMSO (0.5 mM bafilomycin A1, Calbiochem; 10 mM FK506, Sigma) or ethanol (10 mM nigericin, Molecular Probes; 20 mM monensin, Calbiochem). All stock solutions were stored at -20°C.

Current-clamp whole-cell recordings of individually transfected CA3 neurons were performed using a MultiClamp 700B amplifier (Axon Instruments). Recording pipettes (4 - 7 MΩ) were filled with intracellular solution containing (in mM): 135 K-gluconate, 10 HEPES, 4 $MgCl_2$, 4 Na_2-ATP, 0.4 Na_2-GTP,

10 Na_2-phosphocreatine, 3 ascorbate and 0.3 EGTA (pH: 7.3; 295 mOsm). To elicit trains of APs, we applied 3 ms current pulses through the somatic patch clamp electrode and adjusted the amplitude to 0.5 nA above AP threshold (1.5 – 5.5 nA). On-cell recordings of CA3 cell activity were performed in serum-free slice culture medium at a temperature of 35°C (gassed with 95% O_2, 5% CO_2 to a pH of 7.4). Recording pipettes were filled with standard ACSF.

Dissociated hippocampal cells were constantly superfused with a solution containing (in mM) 136 NaCl, 2.5 KCl, 10 mM Hepes, 10 mM D-glucose, 2 $CaCl_2$, 1 $MgCl_2$ (pH 7.4 with NaOH and HCl), 0.01 NBQX, 0.01 *R*-CPP. For weak base calibration, 50 mM NaCl was substituted with NH_4Cl. To stimulate the dissociated cultures, brief current pulses (1 ms, 10-30 mA) were applied to two parallel platinum wires (5 mm apart) using a stimulus isolator (WPI A385, World Precision Instruments). Current amplitudes were chosen by maximizing the change in the green ratio-sypHy fluorescence in response to trains of 40 APs at 30 Hz. All experiments (except on-cell activity recordings: 35 ± 1°C) were performed at 25 ± 1°C by controlling the temperature of the perfusate and the oil immersion condenser (HeatWave-30, Dagan Corp.).

Two-photon imaging

We used a custom-built two-photon laser scanning microscope based on a BX51WI microscope (Olympus) and a pulsed Ti:Sapphire laser (Chameleon XR, Coherent). The laser was tuned to λ = 930 nm to simultaneously excite both the extravesicular tdimer2 and intraluminal pHluorin moieties of ratio-sypHy. Images were acquired with a customized version of the open source software package 'ScanImage' (HHMI, Janelia Farm). Red and green fluorescence was detected through the objective (LUMPlan W-IR2 60×, 0.9 NA, Olympus) and through the oil immersion condenser (1.4 NA, Olympus) using photomultiplier tubes (R3896, H7422P-40, Hamamatsu). We used 725DCXR dichroic mirrors and E700SP blocking filters to reflect emitted photons into secondary beamsplitters, containing 560DCXR dichroic, 525/50 (green) and 610/75 (red) band pass filters (Chroma). For the time-lapse recordings of slices we acquired 50-90 images at a resolution of 64×64 pixels (frame time 128 ms) at 3.3 Hz. Dissociated cells were imaged at a resolution of 128×128 pixels (frame time 256 ms) at 2 Hz. Laser intensity in the back focal plane of the objective was <13 mW. Long-term imaging was performed in standard culture medium using a 25x objective (XLPlan N 25x, 1.05 NA, Olympus) to acquire 512x512 pixels z-stacks of 100 µm depth (voxel

size: 185x185x500 nm). To allow comparison of absolute intensities between day to day imaging sessions, all data was normalized to individual fluorescent microbeads (FluoSpheres 505/515, 0.1 µm) injected into the imaged tissue region via a glass pipette.

Image analysis and display

We analyzed images with custom-written Matlab scripts, using the red channel to automatically detect individual boutons and to adapt the size of rectangular regions of interest (ROIs) to the bouton size. Owing to the full visibility of all ratio-sypHy molecules at rest, this ensures a well defined contribution of post-exocytotic lateral indicator spread (Granseth et al., 2006) to the measured signal, independent of cluster size. ROI length and width were set to 3×σ of Gaussian fits to intensity profiles along the long and short axis of peak intensity-centered hull ellipsoids around automatically segmented blobs (average ROI size 2.2 ± 0.06 × 2.2 ± 0.06 µm). To correct for optical bleed-through, we measured the fluorescence of neurons expressing only tdimer2 and only pHluorin in both color channels and applied the appropriate correction factors. All red (*R*) and green (*G*) fluorescence intensities were corrected for local background, where $G = FG - FG_{bg}$ and $R = FR - FR_{bg}$. *FG* is the raw green fluorescence signal FG_{bg} and FR_{bg} are the raw average signals of background ROIs next to the boutons. Assuming uniform bleach rates for data acquired at constant laser intensity along individual axons, we corrected all data for bleaching by subtracting monoexponential fits *(G = x × e^(-t/τ))* acquired from the average fluorescence time-course of unresponsive boutons (Figure S2A, B). Bleach rates on the green channel were similar for all conditions including dissociated cells (τ = 4.2 ± 0.3 min; p = 0.44, one-way ANOVA).

We show time-series as bleach-corrected normalized fluorescence change, where $\Delta F_{norm} = [(G - G_0) / ((1 - f_{surf}) \times R)] / (G_{max}/R)$. G_0 was determined by averaging the ROI intensities of the green channel over the first 5-9 frames preceding stimulation. *R* was defined as the first point of a monoexponential fit $(R(t) = R_0 \times e^{(-t/\tau)} + c)$ through the entire red fluorescence time course, thus minimizing the influence of measurement noise and bleaching on *R*. f_{surf} is the fraction of surface expressed ratio-sypHy (eq. 1, see below). G_{max}/R, the 'calibration ratio', is the average ratio of a set of 'fresh' (i.e. not previously imaged) boutons under alkalized conditions. The maximal stimulus-evoked change in green pHluorin fluorescence $(\Delta G = G_{stim} - G_0)$ was determined 500 ms after the end of stimulation by fitting the poststimulus decay of the green signal with a single exponential (Figure 1c): $G(t) = G_{stim} \times e^{(-t_{stim+500ms}/\tau)}$. To account for

differences in vesicle cluster size, raw intensity values are displayed as integrated intensities and converted into photon counts by multiplication with the measured average PMT gain: $\Sigma_{photons} = A_{ROI} \times I \times g$, where A_{ROI} is the ROI area (in pixels), I is the average ROI intensity and g is the PMT gain (in pixels/photon). Vesicle cluster size is quantified as integrated surface-corrected red intensity (ΣR_{ves}) and the total amount of released vesicles (synaptic strength) as integrated evoked change in green intensity ($\Delta\Sigma G$).

The time constant for endocytosis (τ) was determined by a single exponential fit starting 500ms after stimulus end ($G_{(t)} = G_{stim} \times e^{(-t_{stim+500ms}/\tau)}$) (also see Figure S2C, D). For global endocytic rates we performed the fit on the average fluorescence change of all axonal averages of a single condition (before normalization), yielding a weighed axonal contribution to the pooled data independent on the number of boutons per cell. For statistical analysis of axonal endocytic rates, fits were performed on the average axonal traces of each cell separately.

Displayed images are averages of 5-10 frames, median-filtered using Image-J (kernel size = 3×3). All green/red image pairs of ratio-sypHy expressing cells are displayed with the same contrast levels. Color-coded ratio images were generated using a Hue/Saturation/Brightness model as described (Vigot et al., 2006). These pixel-by-pixel ratio images were not used for quantitative analysis.

Synaptic localization of ratio-sypHy

Ratio-sypHy was restricted to punctate structures along individual axons and was effectively excluded from the axonal shaft (Figure S1A). To test whether ratio-sypHy was correctly targeted and functional, we used NH_4Cl (50 mM) to equilibrate the pH over all internal membranes to ~7.4 pH (Miesenbock et al., 1998; Roos and Boron, 1981; Sankaranarayanan et al., 2000). We observed a robust increase in the otherwise barely visible green fluorescence (G), consistent with the unquenching of vesicular pHluorin (Figure S1B). As expected, the red fluorescence (R) remained unchanged. Overall, the median difference between the fluorescence emission ratios of different sets of boutons under resting (G_0/R; vesicular pH ~5.6) and alkalized (G_{max}/R; vesicular pH ~7.4) conditions amounted to 317% of the baseline ratio ($\gamma = ((G_{max}/R) - (G_0/R)) / (G_0/R)$ = 3.17, n = 922 boutons). This effective dynamic range was highly variable (interquartile range (IQR) = 4.77), suggesting different levels of ratio-sypHy surface expression at individual boutons. The surface fraction of ratio-sypHy in dissociated cells was not different

from the organotypic slice preparation. (27.7 ± 2.2% vs. 28.1 ± 3.5%, *n* = 8 coverslips, 19 cells, p = 0.65). The calibration ratios reached after NH_4Cl application were similar in both preparations (dissociated cells $G_{max}/R = 0.6 \pm 0.04$, *n* = 8 coverslips, not different from slice $G_{max}/R = 0.6 \pm 0.05$, *n* = 19 cells, p = 0.6517, values corrected for differential absorption of red and green light in hippocampal tissue).

We found that resting surface expression of ratio-sypHy was correlated with the expression level (p = 0.0024, *n* = 19 cells) (Figure S1). Expression levels were estimated by the average integrated red fluorescence intensity normalized to the excitation laser power squared. For single-color pH-sensor proteins, the variable amount of surface expression poses a calibration problem: Surface-stranded protein is unquenched and dominates the green baseline fluorescence (G_0). Therefore, it is not advisable to normalize evoked changes in fluorescence to baseline fluorescence ($\Delta G/G_0$). The red fluorescence (R_0) of ratio-sypHy, on the other hand, is not sensitive to intracellular localization (vesicular vs. plasma membrane) and can thus be used as normalization signal. In addition, R_0 was ~8 times brighter than G_0, reducing photon noise and improving measurement precision.

Rejection criteria

Vesicle clusters were classified as functional or non-functional based on their response to stimulation trains. Automatically detected clusters that responded with a fluorescence ratio change that was smaller than the signal-to-noise ratio (SNR) were considered non-responsive ($SNR = (\Delta G/R) / \sigma(G_0/R) < 1$; 25% ± 4.5% of all clusters, n = 11 cells). We also rejected clusters that showed an absolute evoked ratio change that was higher than the calibration ratio plus one SD of baseline fluctuations ($G_0/R + \Delta G/R > G_{max}/R + \sigma(G_0/R)$). Such implausibly high changes were mostly due to accidental bleaching due to previous light exposure or drift of the preparation during acquisition. This excluded clusters with negative and very high final released fractions, a further 6% ± 4.5% of the responding clusters, n = 11 cells). All ratio values with $G/R > G_{max}/R + 3\sigma(G_{max}/R)$ were considered outliers and were removed (2.7 ± 1.92 % of all ratio values). For the calculation of recycling fractions we excluded unrealistically high recycling fractions (>160%) and defined boutons with recycling fractions lower that 1% as unresponsive. Over all conditions tested this excluded 9% and 11% of the data, respectively. We used the same rejection criteria for both dissociated and slice cultures.

In vivo recordings

Neural activity in CA3 was recorded in rats implanted with a ‚hyperdrive' allowing an independent positioning of 14 tetrodes organized into a circular bundle. Tetrodes were twisted from 17 µm polyimide-coated platinum-iridium wire (90% and 10%, respectively, California Fine Wire Company). Electrode tip impedances were adjusted by platinum plating to 120 – 200 kOhm (at 1 kHz).

Before the surgery the animal was food deprived for 12 hours. Anesthesia was induced by placing the animal into a closed chamber with isoflurane vapour and then injecting Equithesin (pentobarbital and chloral hydrate) intraperitonealy in dose 1 ml per 250 g body weight. Additional anesthesia was applied when breathing and reflexes changed. The Hyperdrive was then implanted above the right dorsal hippocampus at coordinates AP 3.8 mm and ML 3.0 mm relative to bregma. Stainless steel screws and dental acrylic were used to stabilize the implant on the skull. Two of the screws served as hyperdrive ground. The majority of tetrodes were slowly lowered towards CA3 within 2-3 weeks after the surgery in steps of ca. 50 µm while the rat was resting in a flower pot on a pedestal. To maintain stable recordings, electrodes were not moved at all before and during the experiment on a given day. Two of the tetrodes were positioned in corpus callosum (reference) and stratum lacunosum moleculare (EEG), respectively.

Neural activity was recorded while the rat was collecting randomly dispersed food in a rectangular enclosure (60x60 cm, 50 cm high walls) with distinct visual cues on its walls. Black curtains surrounded the apparatus to prevent the animal to see the rest of the room. Signal was recorded differentially against the reference tetrode placed in corpus callosum. Hyperdrive was connected to a multichannel, impedance matching, unity gain headstage and its output conducted through a 82-channel commutator to a Neuralynx data acquisition system with 64 digitally programmable amplifiers. Signal was amplified 3,000–5,000 times and band-pass filtered at 600 Hz–6 kHz. Unit waveforms above individually set thresholds (45-70 µV) were time-stamped and digitized at 32 kHz. Position of the light emitting diodes on the headstage was tracked at 50 Hz to assess the animal's position. For the purpose of this study only data from intervals when the rat's movement speed exceeded 5 cm/sec were used. Broadband EEG from each tetrode was recorded continuously.

Spikes were sorted manually after the experiment using graphical cluster-cutting software (MClust, A.D.Redish). The feature space consisted of two-dimensional projections of multidimensional

waveform amplitudes and energies. Autocorrelation and crosscorrelation functions were used as additional separation tools. Putative pyramidal cells were distinguished from putative interneurons by average rate, spike width and occasional complex spikes.

After the experiment was finished, the rat was overdosed with Equithesin and was perfused intracardially with saline followed by 4 % formaldehyde. Brain coronal sections (30 µm) were stained with cresyl violet. Traces of all 14 tetrode locations were identified. Each tip location was considered as the place in the section before the tissue damage became negligible. Only recordings from tetrodes with their tips in CA3 were used in this study.

The AP timestamp data (in seconds) of the 10 units shown in figure 6 is available for download as supplemental material. We used interval data from unit 1 (seconds 90 – 392) as saturating stimulus (stimulus 2) and data from unit 3 (seconds 440 – 490) as shorter stimulus (stimulus 1).

Supplementary References

Atluri, P.P., and Ryan, T.A. (2006). The kinetics of synaptic vesicle reacidification at hippocampal nerve terminals. J Neurosci 26, 2313-2320.

Bolshakov, V.Y., and Siegelbaum, S.A. (1995). Regulation of hippocampal transmitter release during development and long-term potentiation. Science 269, 1730-1734.

Branco, T., Staras, K., Darcy, K.J., and Goda, Y. (2008). Local dendritic activity sets release probability at hippocampal synapses. Neuron 59, 475-485.

De Simoni, A., and Edwards, F.A. (2006). Pathway specificity of dendritic spine morphology in identified synapses onto rat hippocampal CA1 neurons in organotypic slices. Hippocampus 16, 1111-1124.

Granseth, B., Odermatt, B., Royle, S.J., and Lagnado, L. (2006). Clathrin-mediated endocytosis is the dominant mechanism of vesicle retrieval at hippocampal synapses. Neuron 51, 773-786.

Miesenbock, G., De Angelis, D.A., and Rothman, J.E. (1998). Visualizing secretion and synaptic transmission with pH-sensitive green fluorescent proteins. Nature 394, 192-195.

Pratt, K.G., Watt, A.J., Griffith, L.C., Nelson, S.B., and Turrigiano, G.G. (2003). Activity-dependent remodeling of presynaptic inputs by postsynaptic expression of activated CaMKII. Neuron 39, 269-281.

Roos, A., and Boron, W.F. (1981). Intracellular pH. Physiol Rev 61, 296-434.

Sankaranarayanan, S., De Angelis, D., Rothman, J.E., and Ryan, T.A. (2000). The use of pHluorins for optical measurements of presynaptic activity. Biophysical Journal 79, 2199-2208.

Sorra, K.E., and Harris, K.M. (1993). Occurrence and three-dimensional structure of multiple synapses between individual radiatum axons and their target pyramidal cells in hippocampal area CA1. J Neurosci 13, 3736-3748.

Stoppini, L., Buchs, P.A., and Muller, D. (1991). A simple method for organotypic cultures of nervous tissue. Journal of Neuroscience Methods 37, 173-182.

Vigot, R., Barbieri, S., Brauner-Osborne, H., Turecek, R., Shigemoto, R., Zhang, Y.P., Lujan, R., Jacobson, L.H., Biermann, B., Fritschy, J.M.*, et al.* (2006). Differential compartmentalization and distinct functions of GABAB receptor variants. Neuron 50, 589-601.

Figure S1: Localization of Ratio-sypHy

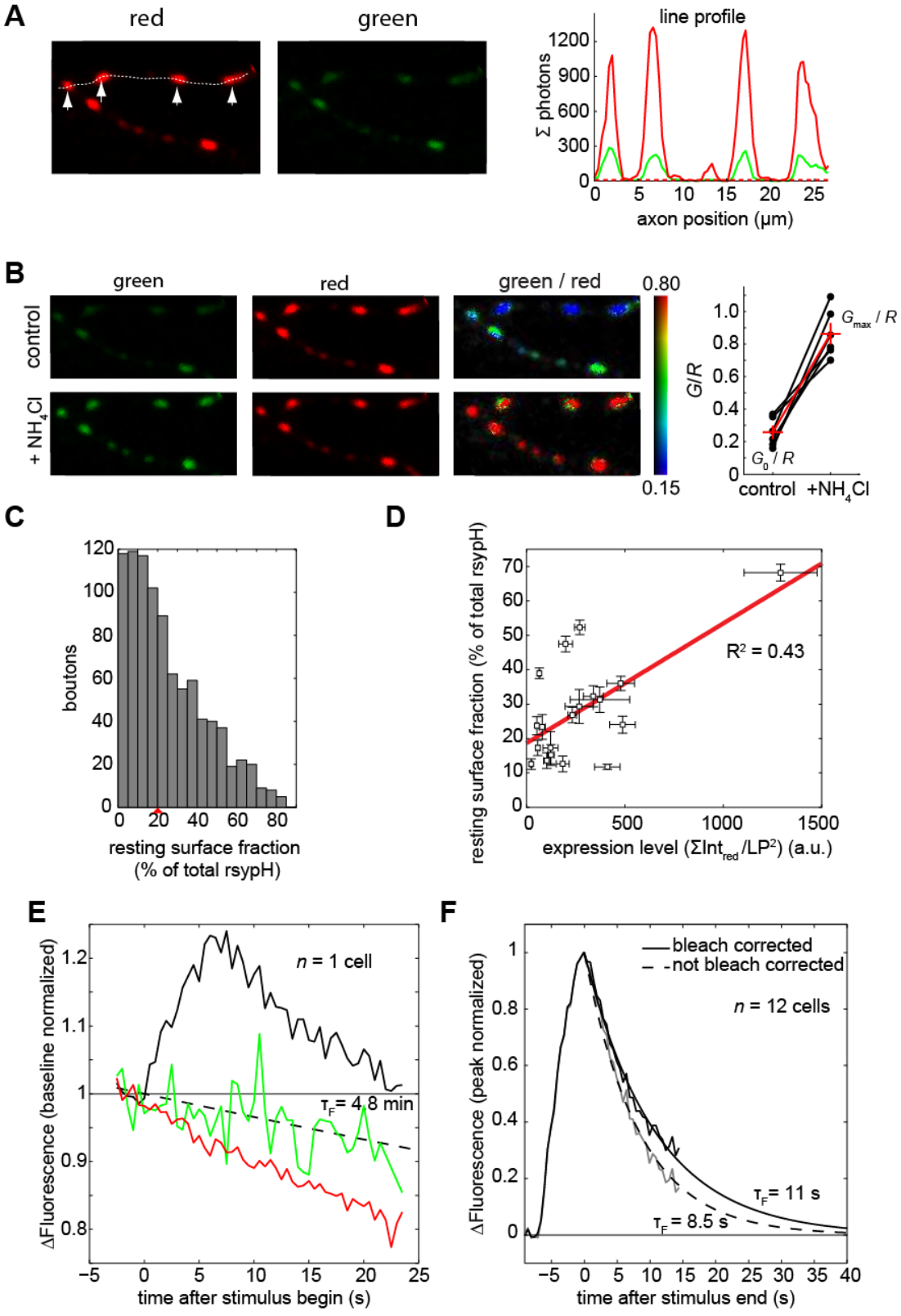

Figure S1: Localization of Ratio-sypHy.

(A) Linearized 3d line profiles through z-stacks of Schaffer collateral (SC) axons were used to assess synaptic localization of fluorescent proteins. Ratio-sypHy showed bright red (tdimer2) and dim green (pHluorin) punctate fluorescence, Axonal shaft was barely detectable.

(B) Alkalization of synaptic vesicles by NH_4Cl (50 mM) resulted in bright green fluorescence. Color-coded green-to-red fluorescence ratio before and after NH_4Cl application is shown (scale bar: 5 µm). Alkalization induced 278 ± 66% relative change in the fluorescence ratio ($\Delta G/R$ / G_0/R) in the 6 boutons displayed (right; all images maximum projection of z-stacks).

(**C**) Distribution of the fraction of ratio-sypHy detected on the bouton surface (n = 922 boutons, 25 slices; red arrowhead: median).

(**D**) Resting surface expression of ratio-sypHy was correlated with expression level ($p = 0.0024$, n = 19 cells). Expression levels were estimated using the average integrated red fluorescence intensity normalized to the excitation laser power squared.

(**E**) Baseline-normalized ratio-sypHy fluorescence traces of responding (SNR $\Delta G/G_0 > 1$, black) and non-responding (SNR $\Delta G/G_0 < 1$) boutons of a single axon as well as red ratio-sypHy fluorescence of the same synapses (red). We fit a single exponential decay through the average time-course of non-responding boutons (dashed black line, τ = 4.8 min) to approximate the average bleach-rate of all boutons along an axon. We correct individual fluorescence traces of responding boutons of a single cell using this rate.

(**F**) Correction for photobleaching results in a prolongation of the uncorrected average poststimulus fluorescence decay time constant by 2.5 s (single exponential fits: dashed line, uncorrected; solid line, corrected). Released fractions derived from the normalized fluorescence traces were only marginally affected by bleach correction (data not shown).

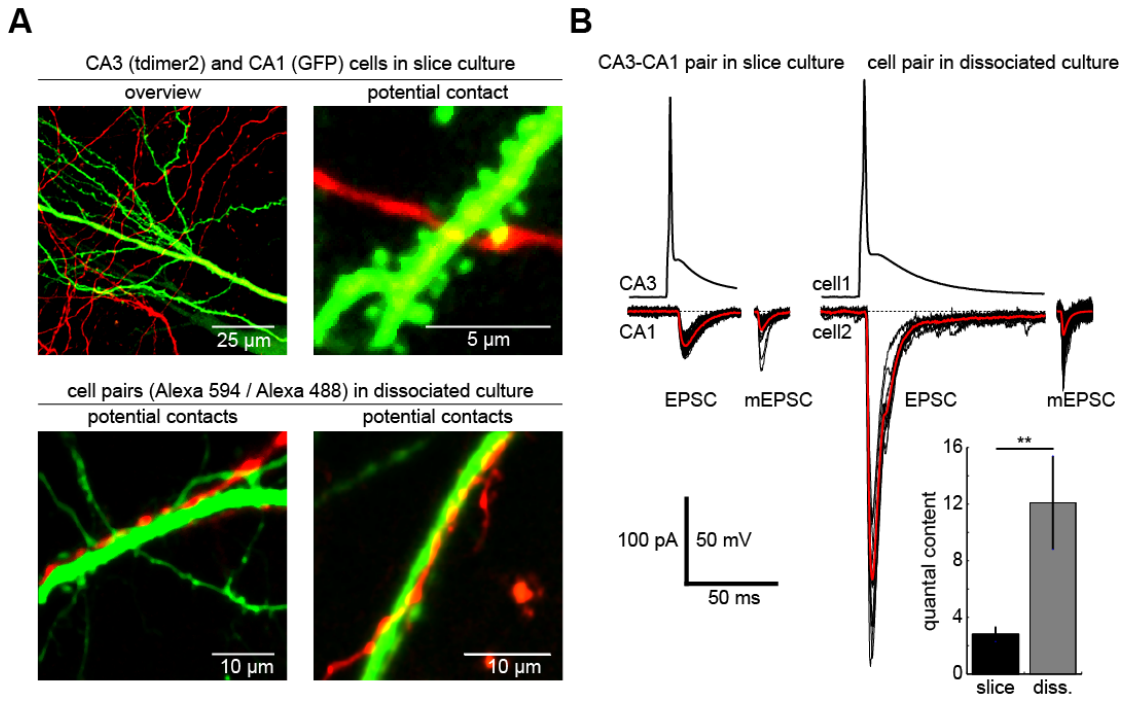

Figure S2: Synaptic topology in dissociated and slice culture

(A) Examples of potential synaptic contacts between CA3 and CA1 cells expressing tdimer2 (red) and GFP (green, upper panels) and of contacts between cells in dissociated cell culture (lower panels) filled with Alexa-Fluor 594 (red) and Alexa-Fluor 488 (green). Multiple neighboring synapses contacting the same target dendrite are typical for dissociated cultures. In contrast, we never observed fasciculation between CA3 axons and CA1 dendrites in slice culture (also see (Sorra and Harris, 1993)).

(B) Dual patch-clamp experiments. APs were evoked in CA3 pyramidal cells in slice culture (left) or in hippocampal cells in dissociated culture (right) by somatic current injection. Evoked unitary excitatory postsynaptic currents (EPSCs) were recorded either in a CA1 pyramidal cell or in a second dissociated cell (voltage clamp, V_m = -65 mV). To assess the average strength of the unitary synaptic connection, EPSC amplitudes are compared to the average amplitude of miniature EPSCs (mEPSCs) measured in another set of cells in slice and dissociated cell culture (recordings in 0.5 µM TTX; mEPSCs in slice cultures were recorded in CA1 pyramidal cells; V_m = -65 mV). Evoked EPSC amplitudes (I) in the CA3-CA1 pairs were ~8 times smaller than in dissociated cell pairs (p = 0.0002). Assuming similar P_r, the EPSC / mEPSC ratio (i. e. current I over 'quantal content' Q, (Pratt et al., 2003)) can be used to compare the number of release sites (N): $I = N \times P_r \times Q$. EPSC / mEPSC ratios were 4.3 times higher in dissociated cells (EPSC/mEPSC = 2.8 ± 0.5 in CA3-CA1 pairs vs. 12.1 ± 3.3 in dissociated cell pairs. P = 0.0027). Thus, depending on the actual value of P_r, CA3-CA1 connections in organotypic cultures formed at least ~3 active synaptic contacts whereas dissociated cells formed at minimum ~12 synapses. These numbers are similar to anatomic estimates of CA3-CA1 connectivity in acute and cultured slices (De Simoni and Edwards, 2006; Sorra and Harris, 1993) and correspond well to paired recordings from acute hippocampal slices (Bolshakov and Siegelbaum, 1995). Furthermore, our estimate of the number of connections in dissociated cultures is comparable to published estimates (Branco et al., 2008; Pratt et al., 2003).

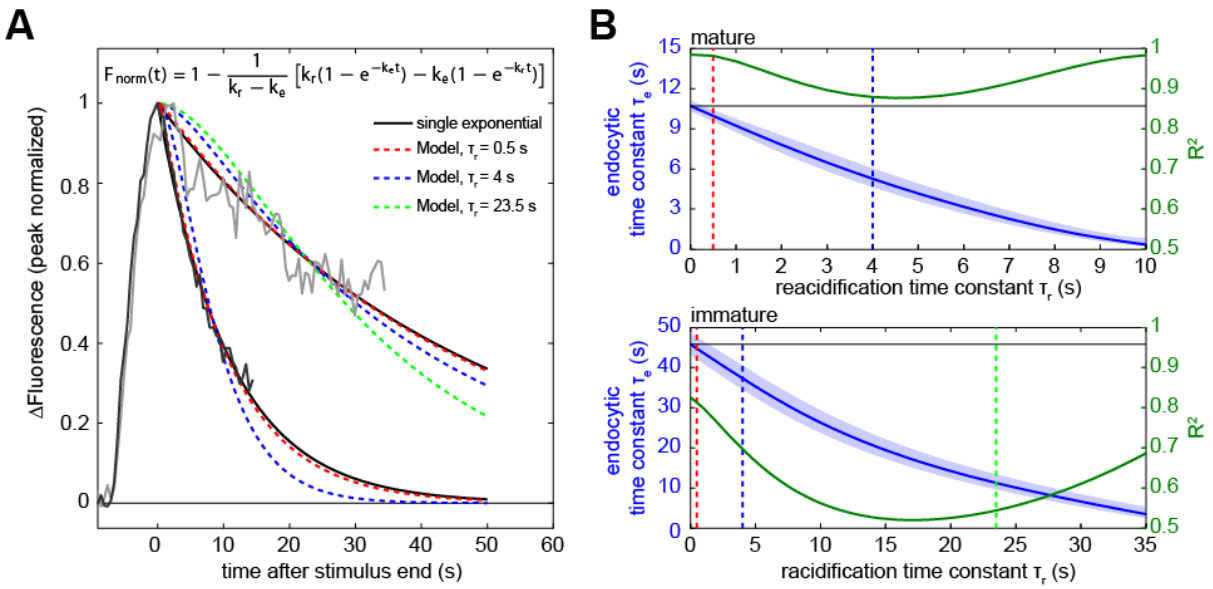

Figure S3: Analysis of ratio-sypHy fluorescence decay

(**A**) Single exponential fits vs. two-step model. Average fluorescence change of mature (black) and immature (gray) SC boutons (bleach-corrected, peak-normalized). We fitted our data with an established model that represents reacidification and endocytosis as two consecutive and irreversible first order kinetic processes (Granseth et al., 2006): $1-(1/(k_r-k_e)) \times (k_r \times (1-\exp(-k_e \times x)) - k_e \times (1-\exp(-k_r \times x))$. The colored lines are best fits to this model with different fixed values for the reacidification rate k_r (0.5 s, red; 4 s, blue; 23.5 s, green), leaving the rate of endocytosis k_e as free parameter.

(**B**) Parameter space of the two-step model for mature (top) and immature (bottom) SC boutons in slice culture. The endocytic time constant, derived from best fits to the model ($\tau_e = 1/k_e$; blue line, shaded area ±95% CI), is plotted against increasing reacidification time constants ($\tau_r = 1/k_r$). R^2 is plotted as a measure of the goodness of fit (green line). Vertical dashed lines correspond to the fits shown in **A.** A good fit was achieved under the assumption of rapid reacidification (τ ~ 0.5 s) under our conditions (25 mM $NaHCO_3$, 25°C). The reported value of τ_r ~ 4 s (Atluri and Ryan, 2006; Granseth et al., 2006) did not match the fluorescence decay at SC boutons in slice culture (dashed blue lines in **A** and **B**). Importantly, a developmental change in reacidification rate is unlikely to explain the difference in fluorescence decay rates in mature and immature SC boutons: If we try modifying the reacidification time constant to change from slow to fast fluorescence decay, we have to accept a much weaker goodness of fit together with $\tau_r > 23.5$ s in immature boutons (dashed green line in **A** and **B**: value of immature τ_r where mature τ_e at τ_r = 0 falls in the 95% CI of immature τ_e), which is not biologically plausible. In conclusion, to avoid overfitting and overestimation of endocytic rates, we used single exponential fits (black lines in **A** and **B**) to extract endocytic time constants from fluorescence decay.

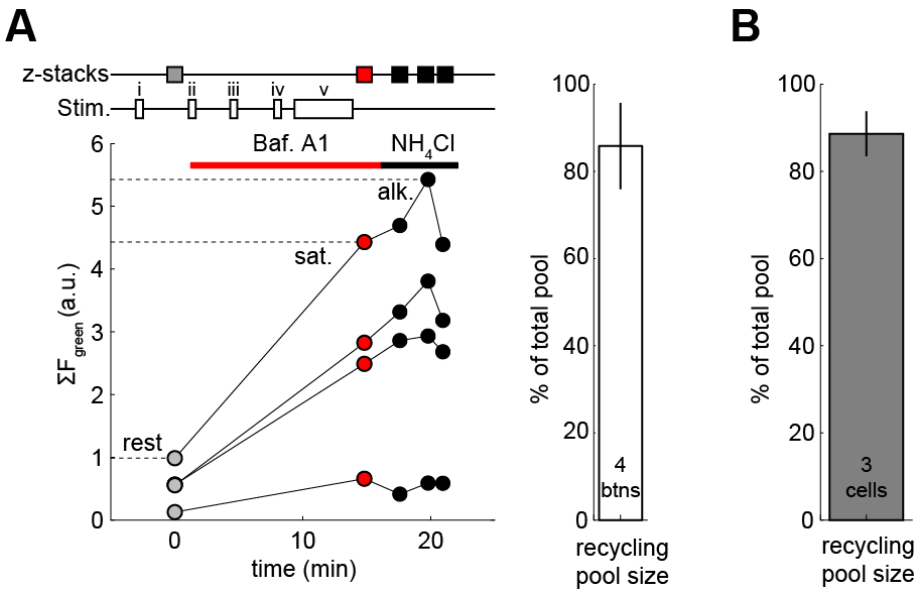

Figure S4: Alkaline trapping experiment at the same set of boutons

(A) Alkaline trapping experiment with repetitive imaging of four boutons of a single axon expressing ratio-sypHy. After confirming axonal stimulation by current injection in CA3 cells (200 AP, 30Hz) (i), a first z-stack was acquired to assess green baseline fluorescence of the boutons. After washin of bafilomycin A1, boutons were monitored in a single z-plane during several stimulations (ii – iii) to confirm the onset of bafilomycin action (iv). This was followed by saturating stimulation (v; 1200 AP, 30Hz). Further z-stacks were taken right after saturation and after NH_4Cl application to assess bouton fluorescence corresponding to full recycling pool turnover and to obtain the peak fluorescence after alkalization of the remaining resting pool. Data shown are peak integrated green fluorescence intensities of individual boutons in z-stacks. Red fluorescence of ratio-sypHy was not evaluated. Resting (rest), saturation (sat.) and alkalization (alk.) fluorescence levels of an individual bouton are indicated by dotted lines (corresponding recycling pool size: 78% of the total pool). Right: average recycling pool size of the cell shown (n = 4 boutons).

(B) Summary of alkaline trapping experiments using repetitive imaging (n = 3 cells, 4 – 10 boutons each).

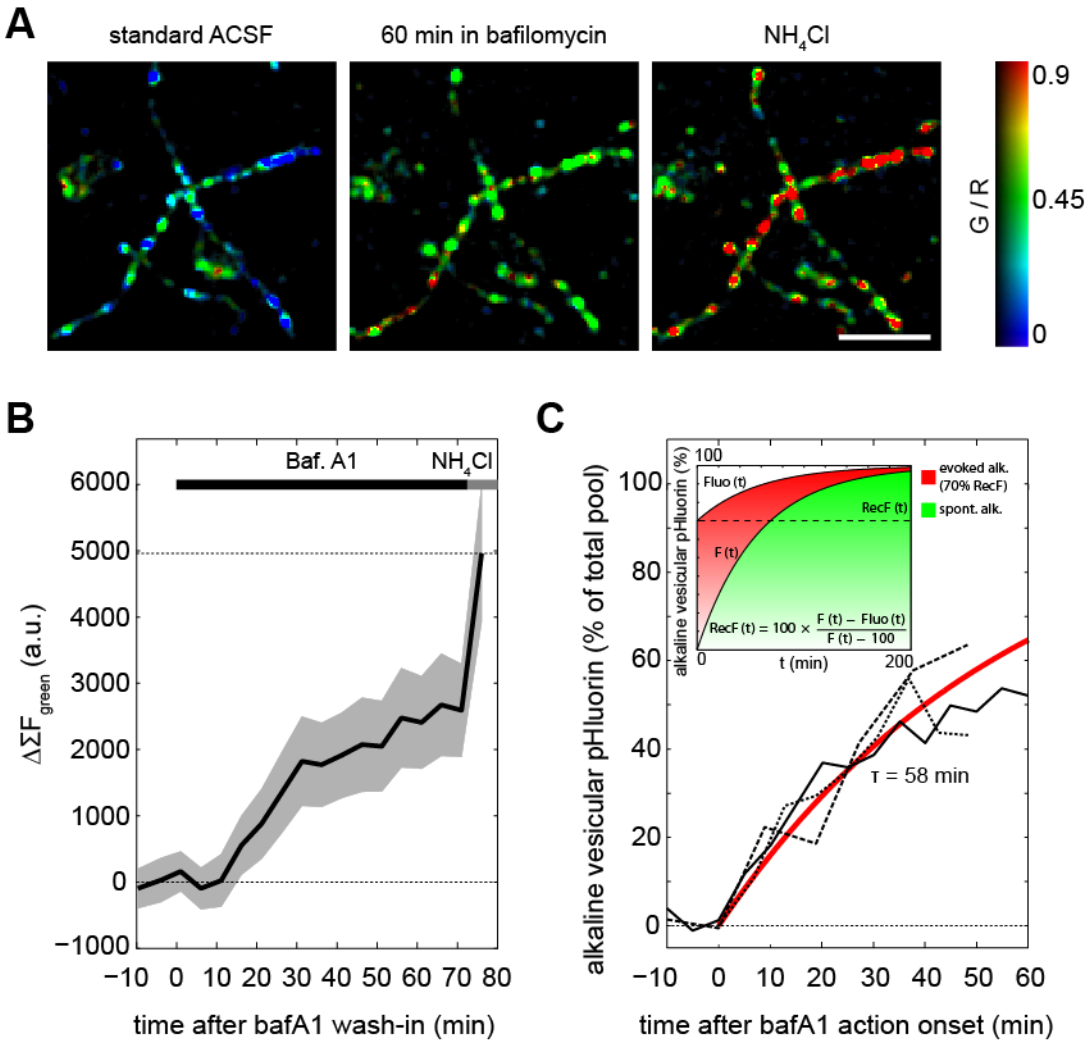

Figure S5: Correction for spontaneous alkalization

(A) Maximum projections of z-stacks of SC boutons expressing ratio-sypHy at rest (left), after 60 min of perifusion with 2 µm bafilomycin A1 (center), and after application of NH_4Cl (right). Scale bar: 10 µm.

(B) Average increase (black trace) in integrated green fluorescence intensity after bafilomycin A1 application (± S.E.M., gray area) for the boutons shown in **A**. In our standard ACSF, spontaneous activity is suppressed using glutamate receptor antagonists but miniature release events and proton leakage across vesicular membranes still lead to a slow increase in pHluorin fluorescence in ACSF containing bafilomycin.

(C) The average spontaneous alkalization rate for 3 sets of boutons of several transfected cells in 3 different slices is reproducible and has a time constant of ~1 h (*F(t) = 100 × 1-e^(-t/τ),* with τ = 58 ± 4.1 min, n=3 slices, 21-73 boutons each). Traces are aligned to the onset of bafilomycin A1 action (last time point before the first detectable increase over baseline fluorescence). The onset of bafilomycin A1 action varied between 3 and 27 min after wash-in (mean: 10.4 ± 2.3 min, *n* = 11 slices) and therefore had to be monitored carefully at 'sentinel boutons' (Figure 5) to minimize the error introduced by spontaneous alkalization or incomplete block of the proton pump. Spontaneous alkalization is not negligible in the case of sequential alkaline trapping using natural stimulation saturation (duration ~15 min from bafilomycin action onset to calibration). We therefore correct all data using the measured spontaneous alkalization rate and the timepoint (t)

of recycling fraction measurement for each bouton relative to bafilomycin action onset at each axon:

The measured alkaline pHluorin fraction (*Fluo(t)*) is the sum of the spontaneous (*F(t)*) and evoked (*E(t)*) pool of alkaline pHluorin:

(1) $Fluo(t) = F(t) + E(t).$

The evoked pHluorin pool is a fraction of the non-alkalized pool (*1-F(t)*) that corresponds to a given recycling pool size (*RecF*):

(2) $E(t) = RecF \times (1-F(t))$.

By combining (1) and (2) we can solve for *RecF* and yield:

(3) $Rec(F) = (F(t) - Fluo(t)) / (F(t) - 1)$

The inset in **C** is a graphical representation of this correction using an assumed recycling pool size of RecF = 70% of the total pool. All experiments were corrected similarly.

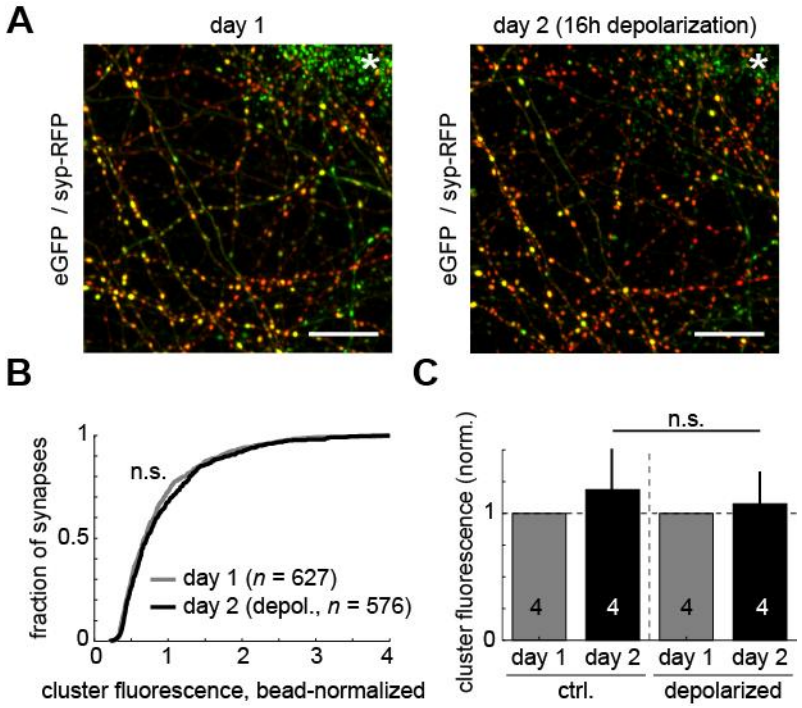

Figure S6: Chronic depolarization does not change total vesicle cluster size.

(A) Boutons in stratum radiatum expressing eGFP and synaptophysin-tdimer2 (syp-RFP) before (left) and after (right) 16 h of incubation under depolarizing conditions (two-photon excitation, maximum projection of z-stacks, depth: 0 - 100 µm, scale bars: 20 µm). Image contrast is normalized to the average intensity of individual fluorescent micro-beads injected into the tissue (asterisks).

(B) In this example, the bead-normalized red intensity of individual syp-RFP$^+$ vesicle clusters was not different after overnight depolarization (p=0.1777, Kolmogorov-Smirnov test).

(C) Summary of long-term imaging experiments. Cluster size after chronic depolarization is not different from control (*n* = 8 slices, 106 - 627 clusters each, p = 0.8857).